AD-A164 781 THREE-DIMENSIONAL SEPARATION AND VORTICAL WAKES OVER A PROLATE SPHEROID..(U) VIRGINIA POLYTECHNIC INST AND STATE UNIV BLACKSBURG DEPT OF E.. D P TELIONIS ET AL. 1/1

UNCLASSIFIED SEP 85 VPI-E-86-1 DTNSRDC/ASED-CR-01-85 F/G 20/4 NL

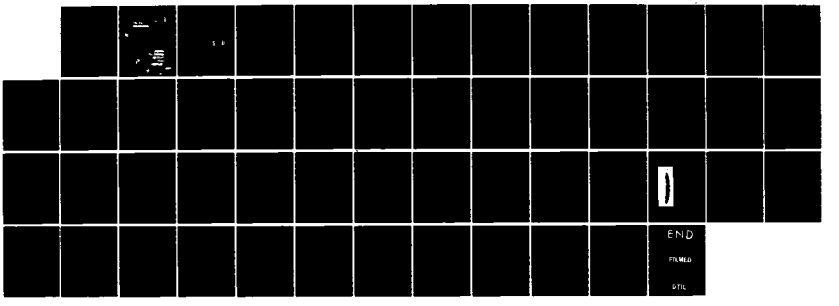

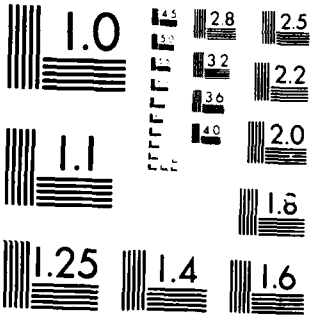

COLLEGE OF ENGINEERING

THREE-DIMENSIONAL SEPARATION AND VORTICAL WAKES OVER A PROLATE SPHEROID

by
D. P. Telionis and C. E. Costis
Department of Engineering Science & Mechanics
Virginia Polytechnic Institute & State University

VIRGINIA POLYTECHNIC INSTITUTE AND STATE UNIVERSITY

DTNSRDC-ASED-CR-01-85

THREE-DIMENSIONAL SEPARATION AND VORTICAL WAKES OVER A PROLATE SPHEROID

by
D. P. Telionis and C. E. Costis
Department of Engineering Science & Mechanics
Virginia Polytechnic Institute & State University

September 1985

Theoretical Phase Report for April 1984 - August 1985

APPROVED FOR PUBLIC RELEASE: DISTRIBUTION UNLIMITED

Prepared for

DAVID W. TAYLOR NAVAL SHIP RESEARCH AND DEVELOPMENT CENTER
Aviation and Surface Effects Department
Bethesda, Maryland 20084

SECURITY CLASSIFICATION OF THIS PAGE (When Data Entered)

REPORT DOCUMENTATION PAGE

READ INSTRUCTIONS BEFORE COMPLETING FORM

1. REPORT NUMBER: DTNSRDC-ASED-CR-01-85	2. GOVT ACCESSION NO.: AD-A164 781
3. RECIPIENT'S CATALOG NUMBER:	
4. TITLE (and Subtitle): THREE-DIMENSIONAL SEPARATION VORTICAL WAKES OVER A PROLATE SPHEROID	5. TYPE OF REPORT & PERIOD COVERED: Final Report
	6. PERFORMING ORG. REPORT NUMBER: VPI-E-86-1
7. AUTHOR(s): Demetri Pyrros Telionis and Christopher Evangelos Costis	8. CONTRACT OR GRANT NUMBER(s): N00167-84-C-0044
9. PERFORMING ORGANIZATION NAME AND ADDRESS: Virginia Polytechnic Institute and State Univ. Blacksburg, Virginia 24061	10. PROGRAM ELEMENT, PROJECT, TASK AREA & WORK UNIT NUMBERS:
11. CONTROLLING OFFICE NAME AND ADDRESS: David W. Taylor Naval Ship R&D Center Aviation & Surface Effects Dept. Bethesda, Maryland 20084	12. REPORT DATE: September 1985
	13. NUMBER OF PAGES: 44
14. MONITORING AGENCY NAME & ADDRESS(if different from Controlling Office):	15. SECURITY CLASS. (of this report): UNCLASSIFIED
	15a. DECLASSIFICATION/DOWNGRADING SCHEDULE:

16. DISTRIBUTION STATEMENT (of this Report)

APPROVED FOR PUBLIC RELEASE: DISTRIBUTION UNLIMITED

17. DISTRIBUTION STATEMENT (of the abstract entered in Block 20, if different from Report)

18. SUPPLEMENTARY NOTES

19. KEY WORDS (Continue on reverse side if necessary and identify by block number)

Three-Dimensional Boundary Layers
Three-Dimensional Separation
Three-Dimensional Wakes
Skin Friction Lines

20. ABSTRACT (Continue on reverse side if necessary and identify by block number)

A vortex-lattice code was developed to generate potential flow solutions over three-dimensional bodies. An approximate boundary-layer technique is incorporated to allow the calculation of the line of separation. The separated vortex sheets are modeled in terms of a vortex grid which is convected with the flow. Special conditions at separation determine the strength of nascent vorticity. Viscous-inviscid interaction in three dimensions allows the accurate prediction of the line of separation and the pressure distribution over the attached flow region.

DD FORM 1 JAN 73 1473 EDITION OF 1 NOV 65 IS OBSOLETE

UNCLASSIFIED

SECURITY CLASSIFICATION OF THIS PAGE (When Data Entered)

Table of Contents

Figures

Abstract

The vortex-lattice method is employed to calculate the inviscid flow and the unsteady development of separated vortex sheets over a prolate spheroid. An approximate boundary-layer method based on the assumption of local similarity is used to calculate the line of open separation. The two schemes interact through the line of separation, which is allowed to displace as the wake grows. The shape of the wake is calculated, and pressure distributions are compared with experimental data. The interaction scheme predicts very accurately the pressure on the attached flow region but displays unexpected spacial variations over the separated region.

1. Introduction

Aerodynamic problems involving massive regions of separated flow in three dimensions can be treated today numerically only by methods of discrete vortex dynamics. Navier-Stokes codes would require incredible amounts of computer time and space to generate the solution to a practical problem. In two dimensions, a variety of problems have been considered using discrete vortex methods; for example, the stability of free-shear layers and the wake structures of thin plates or cornered bodies. More related to the present contribution are works considering the problems of separation over bluff bodies; the most popular case being the circular cylinder.[1-5] In fact, the first efforts to consider separated regions over elongated three-dimensional bodies were based on the cross-flow-plane analogy which employs two-dimensional solutions in cross sections of the body. Two-dimensional methods have been refined to include redistribution of vorticity, models for viscous dissipation, etc.

In three-dimensional problems, one set of such methods is known as "vortex-lattice methods." Problems involving sharp-edge separations have been treated in this way with considerable success for steady[6-9] and unsteady[10-12] flows.

Three-dimensional flows involving separation over smooth surfaces have been considered only very recently. Fiddes[13] expanded on a viscous-inviscid interacting method to solve the problem of three-dimensional separation over a cone. This is an elegant mathematical thesis and a revealing contribution limited to slender body configurations and conical flows.

Thrasher[14] studied the flow over a semi-infinite body with a tangent-ogive nose and cylindrical afterbody. He employed an iteration version of a vortex-lattice scheme to solve the problem and assumed that the separation lines coincided with generators of the body. Almosnino and Rom[15] have considered the flow about a very similar semi-infinite body and employed again an iteration method to achieve convergence of the wake vortices. However, they modeled the separated vortex sheets by only four vortex lines on each side emanating from very narrow segments aligned again with generators of the body.

In all invesitgations of three-dimensional bluff-body separated flows, the body was assumed to be semi-infinite. Moreover, with the exception of the degenerate case considered by Fiddes,[13] all other investigators assume that the position of separation is known and that, in fact, it coincides with a meridional line of axisymmetric bodies. In the present paper, we report on our initial efforts to relax the above restrictions. To this end, we have coupled the potential flow calculations with an approximate method of calculating the three-dimensional boundary layers. Moreover, we considered the unsteady development of the wake and allowed the viscous and inviscid fields to interact. The line of separation over a finite body was readjusted at each time step and was found to tend to the position predicted experimentally for a fully developed flow.

Three-dimensional laminar boundary layers have been calculated by a variety of methods in the past decade. We reference here the most recent contributions of Cebeci et al.,[16] Patel and Baek,[17] Tai,[18] and Ragab.[19] All four papers contain extensive reference to earlier contributions. The present authors have developed an approximate method[20]

which is described briefly here and is employed for the calculation of the separation line.

A significant feature of the flow and a controversial point is the development of open separation lines. This phenomenon was described by Maskell[21] and very recently discussed by Tobak and Peake[22] and Wang.[23] In the present report we reference briefly the evidence of our experimental work in favor of open separation[20] and employ our analytical method which is in agreement with this idea.

2. Potential Flow Calculations

The outer flow and the separated vortex sheet are predicted by the vortex-lattice method. This is based on Biot-Savart's law which stipulates that the velocity vector $\bar{V}$ at position $\bar{r}$ induced by a vortex filament of strength Γ is given by

$$\bar{V}(\bar{r}) = \frac{\Gamma}{4\pi} \int \frac{d\bar{\ell} \times (\bar{r}-\bar{s})}{|\bar{r}-\bar{s}|^3} \tag{1}$$

where the variable $\bar{s}$ is a position vector of points along the vortex line. An equivalent formula for the present application gives the velocity induced by a vortex segment of finite length. With quantities defined in Fig. 1, the velocity is expressed as

$$\bar{V}(\bar{r}) = \bar{e} \frac{\Gamma}{4\pi h} (\cos\theta_1 - \cos\theta_2) \tag{2}$$

where $\bar{e}$ is a unit vector normal to the plane defined by the point of interest and the vortex segment.

The velocity field calculated by the superposition of quantities of this form is irrotational except along the vortex lines which represent singularities of the solution. Appropriate distributions of vorticity

along fixed or moving grids can be used to generate solutions of incompressible flows in two or three dimensions with or without separation. As a test for three-dimensional bluff bodies, we considered three basic problems which accept exact closed-form analytical solutions, readily available for comparison: the flow about (a) a sphere, (b) a prolate spheroid, and (c) a general ellipsoid. To solve these problems, vortex-lattices have been defined with their nodes on the surface of the body as shown in Figs. 2 and 3. The strength of each vorticity segment, usually referred to as branch circulation is denoted by the symbol Γ. Most investigators working in this area[6,7,10-12] express Eq. (2) in terms of the loop circulation, G, around a panel of the vortex lattice. The branch circulation Γ is simply the difference of the loop circulations of its two neighboring panels, G_1 and G_2.

$$\Gamma = G_1 - G_2 \tag{3}$$

The branch circulations thus defined automatically generate a divergence-free vortex sheet, which is a classical property of vorticity.

For convenience of the notation, consider a case of N panels with N unknown loop circulations G_j, $j = 1,\ldots N$. These quantities can be specified by imposing the no-penetration condition at N points on the body. We chose here the "average control points," namely, the centroids of the panels. However, we project these points on the actual surface of the body under consideration. The influence matrix A_{ij} is first constructed. An element of this matrix is the value of the normal velocity at the ith control point due to the vorticity distributed around the jth panel with a unit loop circulation. The no-penetration condition then is simply expressed as

$$\sum_{j=1}^{N} A_{ij} G_j = \bar{V}_\infty \cdot \bar{n}_i \tag{4}$$

where $\bar{V}_\infty$ is the freestream and n_i is the normal to the body at the point i. The flowfield about the body under consideration can be generated by solving the system of equations for the quantities G_j.

Typical results obtained by such calculations are shown in Figs. 4 and 5 where we compare the velocity distribution along a meridional calculated by the exact method and the vortex lattice method. The results displayed in these figures correspond to an optimum choice of panel dimensions. Surprisingly, the accuracy of the calculation is improved by adding elements in the axial direction alone. Excellent results were obtained, for example, with 27 panels in the axial direction and only 6 or even just 4 in the circumferential direction.

Separated flows can be calculated by approximating the separated vortex sheets again by vortex lattices.[13-15] This is discussed in detail in Section 4. In the present case we chose to consider impulsively started flows. The steady state will then be obtained as a limit for large times. At present, and mostly due to limitations in computing time, we have not obtained large-time solutions. However, the present results display some very encouraging characteristics.

The Kelvin-Helmholtz theorem dictates that vorticity be transported with the local velocity. This condition automatically generates a force-free wake and is used here in a manner similar to the one described in earlier references.[10-12] The main difference here is that the wake is initiated along a line of separation which is determined by a viscous calculation and is free to readjust at each time step.

The shed vorticity in the form of two rows of panels at the root of the separated vortex sheets are determined at each time step from viscous-inviscid interaction as described in Section 4. In the next time

step this row of panels is convected away from the body and a new row of panels is generated in the same way. The free vortex panels must be accounted for in the calculation of the velocity field. Equation (4) must be modified to include $\bar{V}_w$, the velocity induced by the wake

$$\sum_{i=1}^{N} A_{ij} G_j = (\bar{V}_\infty + \bar{V}_w) \cdot \bar{n}_i \qquad (5)$$

It should be noted that the matrix A_{ij} is universal for a certain body configuration, but the calculation of the velocity $\bar{V}_w$, although tedius and time consuming, must be repeated at each time step. Finally, the system of Eqs. (5) is nonsingular and can be solved with the same routine used to solve Eqs. (4).

3. Boundary-Layer Calculations

The boundary layer was calculated by an approximate method developed earlier by the authors[20] and repeated here for completeness. The method is based on the assumption that the boundary-layer flow over a general body is locally similar to the flow over a special body whose solution is readily available. Such bodies are cylinders of arbitrary cross section at yaw with respect to the oncoming flow.

Consider the flow about a cylinder in yaw. Let the x, y, and z axes be parallel to the generators, along the contour of the body and perpendicular to the generators, and normal to the body, respectively (see Fig. 6a). Let u, v, and w be the corresponding velocity components, and U_∞, V_∞ the components of the undisturbed freestream. The governing equations in their dimensionless stretched form then read

$$\frac{\partial v}{\partial y} + \frac{\partial w}{\partial z} = 0 \tag{6}$$

$$v \frac{\partial u}{\partial y} + w \frac{\partial u}{\partial z} = \frac{\partial^2 u}{\partial z^2} \tag{7}$$

$$v \frac{\partial v}{\partial y} + w \frac{\partial v}{\partial z} = V \frac{dV}{dy} + \frac{\partial^2 v}{\partial z^2} \tag{8}$$

Notice that there is no pressure gradient term in Eq. (7). Moreover, Eqs. (6) and (8) can be solved independently of Eq. (7). The familiar boundary conditions are

$$u = v = w = 0 \qquad \text{at } z = 0 \tag{9}$$

$$u \to U \,, \; v \to V \qquad \text{as } z \to \infty \tag{10}$$

For an outer flow given by

$$U = U_\infty \tag{11}$$

$$V = C_1 y + C_3 y^3 \tag{12}$$

the solution was obtained in the form of two-term expansions

$$u = U_\infty \left[g_0(z) + \frac{C_3}{C_1} y^2 g_2(z) \right] \tag{13}$$

$$v = C_1 y \, f_1(z) + C_3 y^3 \, f_3(z) \tag{14}$$

and the functions f_1, f_3, g_0 and g_2 were tabulated.[24]

According to our method, the rules of correspondence between points on the body of interest and a Sears body required matching of the following:

a. the reduced distances x along inviscid streamlines scaled with the total length of each streamline,

b. the U velocity component,

c. the V velocity component, and

d. the velocity gradient along the inviscid streamline.

For a coordinate system x,ϕ defined on a prolate spheroid as shown in Fig. 6b, the four conditions read

$$x = x_s \tag{15}$$

$$v(x,\phi) = C_1 x_s + C_3 x_s^3 \tag{16}$$

$$u(x,\phi) = V \tag{17}$$

$$\frac{\partial(u^2 + v^2)}{\partial s} = C_1 + 3C_3 x_s^2 \tag{18}$$

where x_s is the reduced distance along the Sears body.

Equations (15)-(18) are solved at each point on the body of interest for the quantities x_s, C_1, C_3, and V. They thus define a Sears body and determine a point on this body. The solution at this point is then given by Eqs. (13) and (14) and is assumed to hold at the corresponding point on the body of interest.

The direction of the skin friction on the surface of the body was calculated in this way at the control points of the vortex lattice method. A computer program was prepared for the calculation of skin firction lines and boundary-layer edge streamlines. Integration was started at points equally spaced on a meridional line and was marched in both the upsteam and downstream direction. In this way difficulties encountered in the neighborhood of stagnation points were avoided. In fact, the method provides a clear indication of accuracy at stagnation

points where it was demonstrated that all lines pass within a distance of a/1000 of each other.

4. Viscous-Inviscid Interaction

In the present problem we allow the boundary layer to interact with the outer flow only through separation. The stength of the vorticity shed at separation and the location of the line of separation control the development of the free vortex sheets which roll up forming the wake. The structure of the flow at separation and the mathematical modeling that allows the two solutions, the viscous and the inviscid to interact with each other is of crucial importance.

The topology of skin friction lines has been studied extensively in three-dimensional boundary layer flows. Experimental evidence and numerical information indicate that the skin friction lines merge together along the line of separation. Recent careful boundary-layer calculations[16] point to the direction that the separation line is an evelope of skin friction lines and therefore, within the framework of uninteracted boundary-layer theory, a singular behavior should be expected there. Thus, it is justified to use the Sears model for the construction of local-similarity solutions, since it is also singular along the line of separation.

It is well known that the vortex lines on the surface of the body are orthogonal to the skin friction lines. This implies that the surface vortex lines meet the line of separation at an angle of 90° and lift off the body surface also perpendicular to the line of separation. Incidentally, this is contrary to the common concept of two-dimensional separation where, in principle, surface vortex lines are parallel to the

line of separation. The authors and their associates have obtained some experimental evidence that in two-dimensional flows, well-organized cells of cross flow are present in the neighborhood of separation. It is therefore possible that all separation lines are lines of zero vorticity. The picture described above is actually the limit of the behavior of streamlines and vortex lines as the distance from the wall tends to zero. Actually, the total amount of vorticity parallel to the lines of separation is not at all zero at separation. In fact, it is the dominant portion of the vorticity that the boundary layer sheds in the wake.

A straightforward integration of vorticity across the boundary layer indicates that, within the boundary-layer approximation, the magnitude of the vorticity flux at a station of the boundary layer is proportional to the square of and its direction is normal to the direction of the edge velocity. This fact has been employed extensively in investigations of two-dimensional flows and was lucidly explained again by Sears.[25] The idea is that in approximating the shed vorticity by discrete potential vortices, as shown schematically in Fig. 7a, the strength of the nascent vortices must be compatible with the vorticity contained in the boundary layer. For a straightforward derivation of the classical formula, consider the circulation about the loop ACOO' shown in Fig. 7b.

$$\Gamma = \oint \bar{V}\cdot d\bar{\ell} = \iint \bar{\Omega}\cdot d\bar{A} \qquad (19)$$

For steady flow, the time derivative of the integral on the right-hand side vanishes, except for a contribution along the side OO', which allows vorticity to be convected outside of this domain.

$$\frac{d\Gamma}{dt} = \int_0^{\delta} u\Omega dy \tag{20}$$

And within the boundary-layer approximation, $\Omega \sim \partial u/\partial y$ and, hence,

$$\frac{d\Gamma}{dt} = \frac{1}{2} U_e^2 \tag{21}$$

where U_e is the velocity at the edge of the boundary layer. This condition is extended below for three-dimensional flows and is employed to calculate the strength of the nascent vortices at each time step.

Consider a three-dimensional boundary layer over a solid surface aligned with the coordinate plane xy. In the notation of Fig. 8 then the flux of vorticity can be represented by two components which can be obtained by similar integrations across the boundary layer

$$\frac{d\Gamma_x}{dt} = \frac{1}{2} U_e^2, \qquad \frac{d\Gamma_y}{dt} = \frac{1}{2} V_e^2 \tag{22}$$

What is of great importance and interest here is that nascent vorticity is parallel to the wall but not necessarily parallel to the line of separation. This is because by definition the vorticity vector in an attached boundary layer is parallel to the wall. The vorticity vector, therefore, is normal to the edge velocity which in turn is <u>not</u> normal to the line of separation. If we need to discretize the nascent vorticity, then we can simply resolve it in components parallel and perpendicular to the line of separation but always parallel to the surface of the body, as shown schematically in Fig. 8. Let the plane yz in this figure be a plane of separation. Since vorticity is convected with the flow, the vorticity vector $\Delta\Gamma_y$ is turned to align itself with

the flow direction, as shown again in Fig. 8. This condition was implemented in the numerical scheme employed here.

A discretization scheme of the free vortex sheet originates with a ribbon with rectangular elements. The surface of the ribbon was assumed to be parallel to the surface of the body at an arbitrary distance of 0.2R where R is radius of the cross section of the body at the station under consideration. More properly, this distance should be a length proportional to the displacement thickness of the boundary layer. The outer nodes of the ribbon were allowed to be convected and a new ribbon of vorticity was generated according to the above scheme. In this way a free vortex sheet was generated.

5. Results & Discussion

Two types of problems were solved with the codes developed here. The initial condition for both problems was the potential flow about the body. In the first problem we assumed that the boundary layer dev 'ops in a quasi-steady way but the vortex sheets develop in time and grow, feeding their influence back into the freestream and the boundary layer. In this formulation we allow the line of separation to relax and relocate. This is therefore an interactive method. In the second problem we specify the line of separation either arbitrarily, or we use experimental data; for example, the data of Meier et al.[27] No boundary layer solution is then necessary. However, the solution is again developed iteratively, by allowing the vortex sheet to grow as time increases.

The first solution was constructed as follows. A set of skin friction lines based on the exact potential flow solution was calculated

first. For a prolate spheroid with axes ratio 1:4, the result is shown in Fig. 9a. The strength of the nascent vortices was then calculated and allowed to drift with the local velocity. The inviscid flow problem, namely Eqs. (5) were solved again to determine the new loop circulations on the body. With the updated potential flow, a new set of skin friction lines was calculated to determine a new envelope, namely the new position of the line of separation. Once again the stength of the nascent vortices was calculated. The free vortices were then convected again by increments proportional to the local velocities. The process was then repeated for a total of six time steps.

Figures 9b-e display the development of the vortex sheet after the thrid and through the sixth time step for a prolate spheroid at an angle of attack of $\alpha = 30°$, started impulsively from rest. In these plots, the thick lines on the body are the skin friction lines, and the thin lines are the inviscid streamlines. The line of separation is clearly identified in all figures as an envelope of the skin friction lines. The separated vortex sheets are shown in the form of a grid which at the nth time step is made up of n ribbons.

It is clearly desirable to allow the calculation to march to higher values of time. It is believed that six time steps are not enough for the full development of the wake. However, at larger time steps numerical instabilities develop which destroy the smoothness of the wake. Figure 10 displays the displacement of the line of separation as the flow interacts with the boundary layer. It is seen that a boundary layer calculation based on the potential outer flow predicts very early separation in the forward portion of the body. This is the universal finding of researchers who employed a wide variation of boundary-layer

calculations as shown in Fig. 11. It should be noted that our simple method for the calculation of a three-dimensional layer with a potential, unseparated outer flow is in excellent agreement with many other complex methods.

In Fig. 12 we display the direct comparison of flow visualizations with our calculation. The streaklines in this figure were obtained by dyes released in the windward side of the model.[20] The dyes are aligned more or less with the skin friction lines. Moreover, they turn sharply along the line of separation and lift off along the vortex sheet. It should be emphasized here that the first vortex line, the nascent vortex, is located at a distance 0.2R above the body. As a result, viewed perspectively from an angle of $\phi = 90°$, the vortex line is projected on the separation line only if its polar coordinate is $\phi = 90°$. For larger ϕ's, there is a discrepancy proportional to $(0.2R)\sin\phi$, as shown schematically in Fig. 13. This explains partially the deviation in Fig. 12 between the vortex line and the separation line at the leading part of the body, where both curves tend to the windward side, i.e., larger values of ϕ.

A few other configurations were tested with our interactive code as well. Here we present two examples: an ellipsoid with axes ratios 1:6:4 and a projectile shape. Results for the ellipsoid at angle of attack of $\alpha = 30°$ are displayed in Fig. 14, representing the first instant as well as the fifth time step after the impulsive start. In Fig. 15, we show the results of the interactive code for the flow over an ogive-cylinder body at an angle of attack $\alpha = 24.5°$. Figure 16 displays resuls for the same body but with a line of separation fixed at the $\alpha = 90°$ meridional. At the bottom of this figure, we present the calculated vector fields at two cross-sectional planes.

To facilitate comparison with the experimental results of Meier et al.,[26] it was necessary to prescribe the line of separation because their boundary layers were turbulent and our approximate code cannot handle this situation. The calculated wake is shown in Fig. 17, while in Fig. 18 we present a comparison between the analytical and the experimental velocity fields at a cross section of the flow. Apparently the vortex sheet has not developed enough after six time steps. The experimental field indicates larger velocities in the vortex as well as a vortex core which is situated a little closer to the plane of symmetry.

A tape with the pressure distributions measured by Meier and his group has been available in the United States and was employed by other investigators as well for comparison. In Fig. 19 we display along two meridionals the experimental data obtained from the tape and the present numerical results. In the same figure, the potential flow results are shown.

Our analysis indicates that it is very hard to predict with a discrete-vortex method the pressure distribution undeneath the separated flow region. Apparently the wake vortices break down quickly into turbulence which smooths out the pressure signature on the body. This became more obvious when we plotted our predicted distribution as a function of the azimuthal angle. Another reason for this failure could be the limitation in the size of the grid and the number of vortex lines which make up the wake. An example of pressure distribution at $x/L = 0.4812$ is shown in Fig. 20. However, this relatively good agreement could not be reproduced at all stations and was found to depend upon the size of the time step.

It is believed that the method can provide reliable results for the flow and pressure distribution over the attached flow region. However, the base pressure, which incidentally varies with the length of the body, can also be predicted simply by assuming that from separation and on to the leeward side, the pressure is uniform and equal to its value at separation. Results calculated in this way contrasted with experimental data are shown in Figs. 21 through 24.

Conclusions

The present calculations have further demonstrated the potential of the vortex-lattice method. For the first time, a boundary layer solution, although somewhat crude, was coupled with the vortex-lattice solution to determine the location of separation and its displacmenet in time as the wake grows and rolls up. It was demonstrated that the strength of the shed vortex can be determined by simple approximate formulas which essentially represent integrals of boundary-layer profiles. The code we developed is not limited to the configuration considered here. In fact, viscous solutions already have been generated for a variety of ellipsoids with different axes ratios.

Acknowlegment

This work was supported by the Naval Air Systems Command administered by David Taylor Naval Ship R&D Center, under Contract No. N00167-84-K-0044. The continuous interest and meaningful advice of the contract monitor, Dr. T. C. Tai, is particularly appreciated.

References

1. Gerrard, J. H., "The Mechanics of the Formation Region of Vortices Behind Bluff Bodies," Journal of Fluid Mechanics, Vol. 25, Jun. 1966, pp. 401-411.

2. Sarpkaya, T., "An Analytical Study of Separated Flow About Circular Cylinders," Journal of Basic Engineering, Vol. 90, Dec. 1968, pp. 511-520.

3. Deffenbaugh, F. D. and Marshall, F. J., "Time-Development of the Flow About an Impulsively Started Cylinder," AIAA Journal, Vol. 14, Jul. 1974, pp. 908-913.

4. Kuwahara, K., "Study of Flow Past a Circular Cylinder by an Inviscid Model," Journal of the Physical Society of Japan, Vol. 45, Oct. 1978, pp. 292-297.

5. Sarpkaya, T. and Schoaff, R. L., "Inviscid Model of Two-Dimensional Vortex Shedding of a Circular Cylinder," AIAA Journal, Vol. 17, No. 11, Nov. 1979, pp. 1193-1200.

6. Mook, D. T. and Maddox, S. A., "Extension of a Vortex-Lattice Method to Include the Effects of Leading-edge Separation," Journal of Aircraft, 11, No. 2, Feb. 1974, p. 127-128.

7. Kandil, O. A., Mook, D. T. and Nayfeh, A. H., "A New Convergence Criterion for the Vortex-Lattice Models of Leading Edge and Wing-tip Separation," NASA-SP-405 (Vortex-Lattice Utilization Workshop), 1976, pp. 285-300.

8. Zorea, C. R. and Rom, J., "The Calculation of Nonlinear Aerodynamic Characteristics of Wings and Their Wakes in Subsonic Flow," Israel Journal of Technology, 16, 1978, pp. 83-96.

9. Belotserkovskii, S. M., "Gust Effects on Wings of Complex Planforms at Subsonic Speeds," Mekanika Zhrdkosti i Craza, 4, 1966, pp. 129-138.

10. Atta, E. H., Kandil, O. A., Mook, D. T. and Nayfeh, A. H., "Unsteady Flow Past Wings Having Sharp Edge Separation," NASA SP-405, (Vortex-Lattice Utilization Workshop), 1976, pp. 407-418.

11. Thrasher, D. F., Mook, D. T., Kandil, O. A. and Nayfeh, A. H., "Application of the Vortex-Lattice Concept to General, Unsteady Lifting Surface Problems," AIAA Paper No. 77-1157, 1977.

12. Levin, D. and Katz, J., "A Vortex-Lattice Method for the Calculation of the Nonsteady Separated Flow Over Delta Wings," AIAA Paper No. 80-1803, 1980.

13. Fiddes, S. P., "A Theory for the Separated Flow Past a Slender Elliptic Cone at Incidence," RAE Tech Memo 1858, 1980.

14. Thrasher, D. F., "Application of the Vortex-Lattice Concept to Flows with Smooth-Surface Separation," 14th ONR Symposium on Naval Hydromechanics, Univ. of Michigan, Natl. Acad. Press, pp. 1089-1134.

15. Almosnino, D. and Rom, J., "Calculation of Symmetric Vortex Separation Affecting Subsonic Bodies at High Incidence," AIAA Journal, Vol 21, 1983, pp. 398-406.

16. Cebeci, T., Khattab, A. K., and Stewartson, K., "Three-Dimensional Laminar Boundary Layers and the OK of Accessibility," Journal of Fluid Mechanics, Vol. 107, 1981, pp. 57-87.

17. Patel, V. C. and Baek, J. H., "Calculation of Boundary Layers and Separation on a Spheroid at Incidence," in Numerical & Physical Aspects of Aerodynamic Flows, ed., T. Cebeci, 1983; also, AIAA Journal, Vol. 23, No. 1, Jan. 1985, pp. 55-63.

18. Tai, T. C., "Determination of Three-Dimensional Flow Separation by a Streamline Method," AIAA Journal, Vol. 19, No. 10, Oct. 1981, pp 1264-1271.

19. Ragab, S. A., "A Method for the Calculation of Three-Dimensional Boundary Layers with Circumferential Reversed Flow on Bodies," AIAA-82-1023, 1982.

20. Telionis, D. T. and Costis, C. E., "Three Dimensional Laminar Separation," VPI & SU Engineering Report, No. VPI-E-83-4, Dec. 1983.

21. Maskell, E. C., "Flow Separation in Three Dimensions," RAE Aero Report 2565, 1955.

22. Tobak, M. and Peake, J., "Topology of Three-Dimensional Separated Flows," Annual Reviews of Fluid Mechanics, Vol. 14, 1982, pp. 61-85.

23. Wang, K. C., "New Developments About Open Separation," S.D.S.U. Engineering Report, AE&EM TR-82-02, Jul. 1982.

24. Sears, W. R., "The Boundary Layers of Yawed Cylinders", Journal of Aeronautical Sciences, Vol. 15, No. 1, 1942, pp. 49-52.

25. Sears, W. R., "Unsteady Motion of Airfoils with Boundary-Layer Separation," AIAA Journal, Vol. 14, No. 2, 1976, pp. 216-220.

26. Meier, H. U., Kreplin, H.-P., and Vollmers, H., "Velocity Distributions in 3-D Boundary Layers and Vortex Flows Developing on an Inclined Prolate Spheroid," DFVLR-AVA-REPORT IB 222 81 CP 1, 1981.

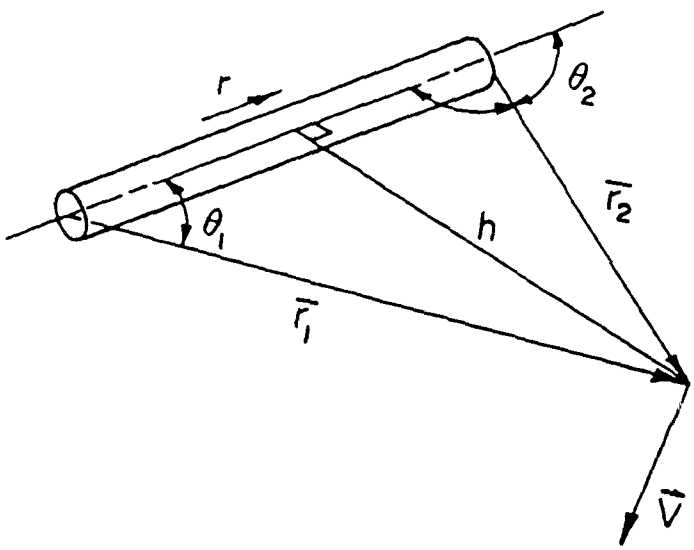

Fig. 1 Velocity induced at a point due to a vortex segment.

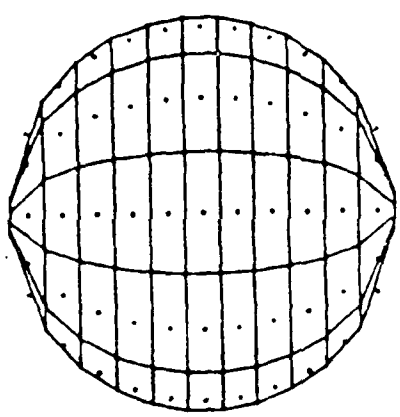

Fig. 2 Vortex lattice and control points for a sphere (10 circumferential and 11 axial panels).

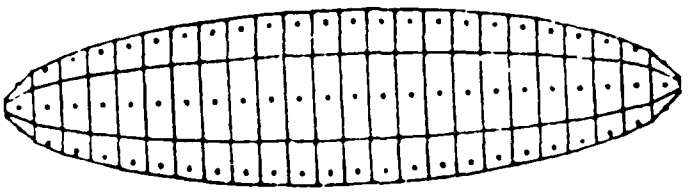

Fig. 3 Vortex lattice and control points for an ellipse with axes ratio 1:4 (6 circumferential and 25 axial panels).

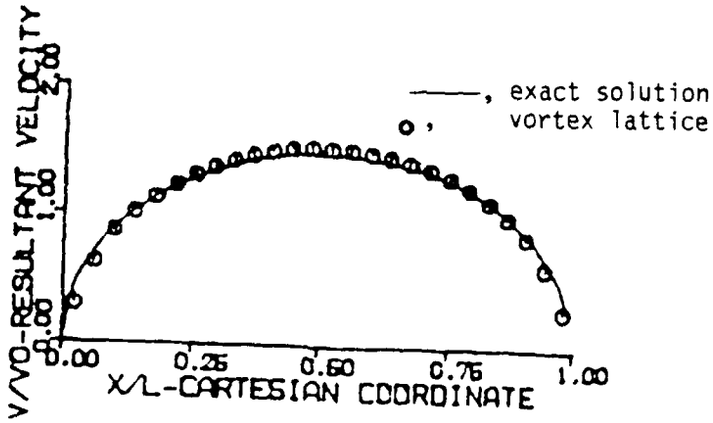

Fig. 4 Velocity distribution along the meridional of a sphere. The vortex lattice had 6 circumferential and 27 axial panels.

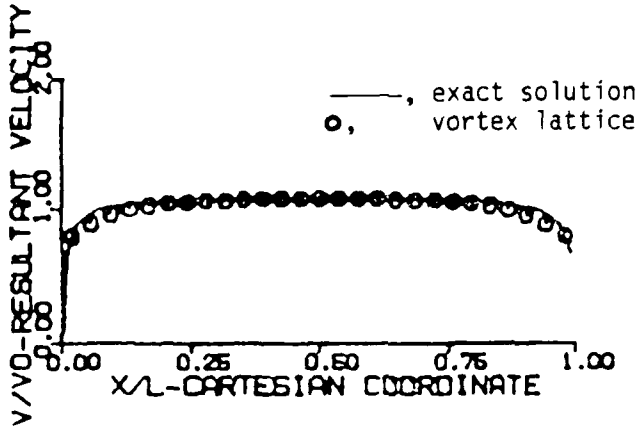

Fig. 5 Velocity distribution along the meridional of a prolate spheroid at zero angle of attack. The vortex lattice had 4 circumferential and 28 axial panels.

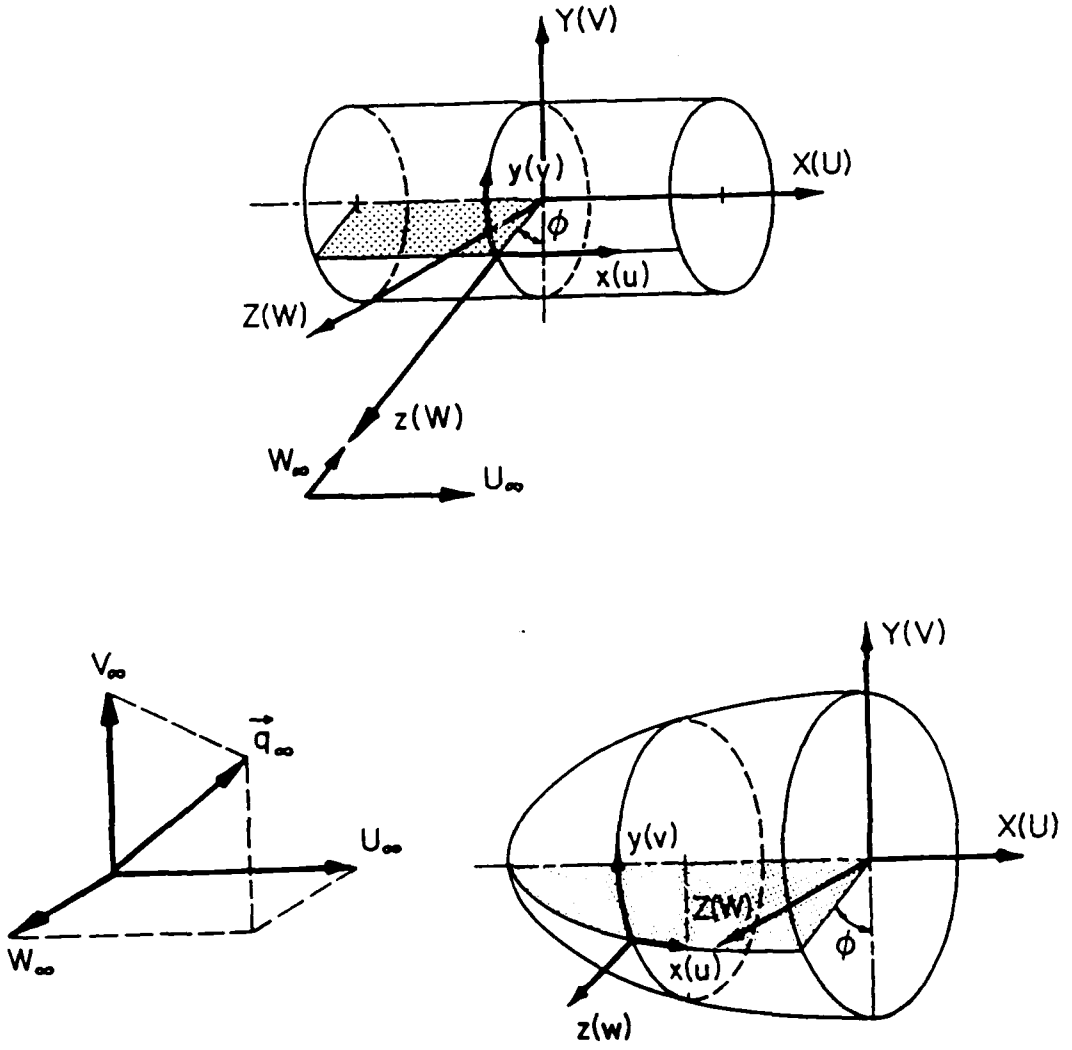

Fig. 6 Coordinate system for boundary layer calculations.

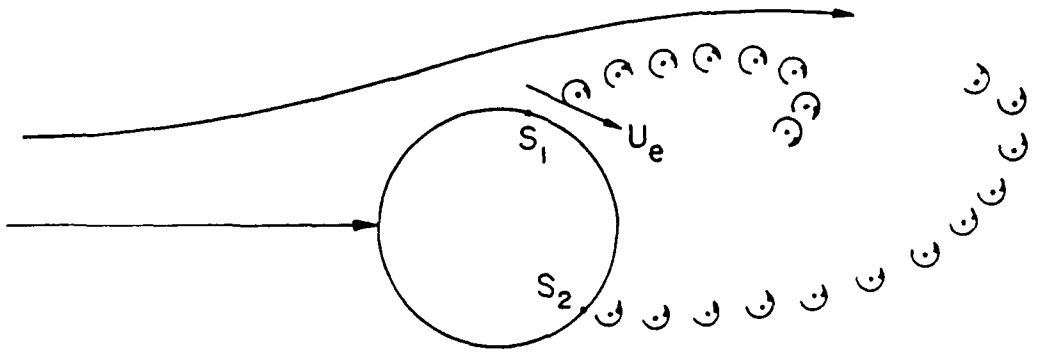

Fig. 7a Schematic of discrete vortex shedding at separation points S_1 and S_2.

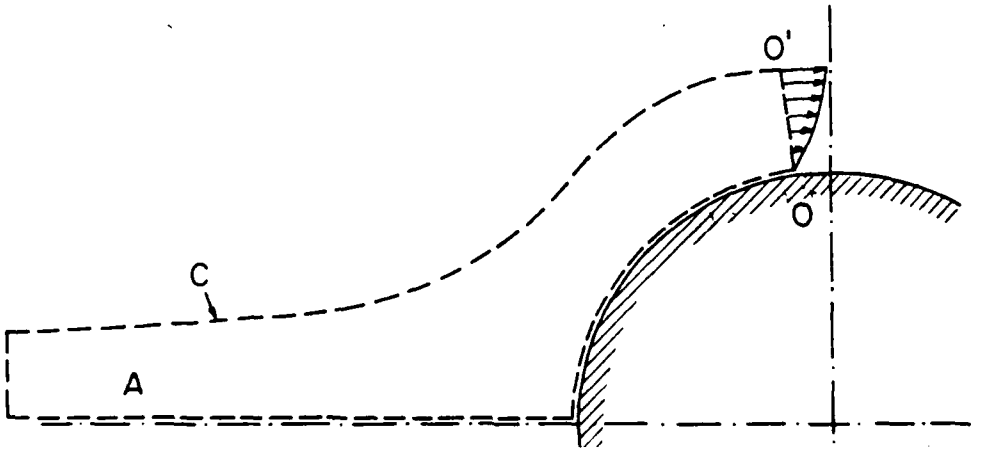

Fig. 7b Contour of integration for the circulation.

Fig. 7 Vorticity field in two dimensions.

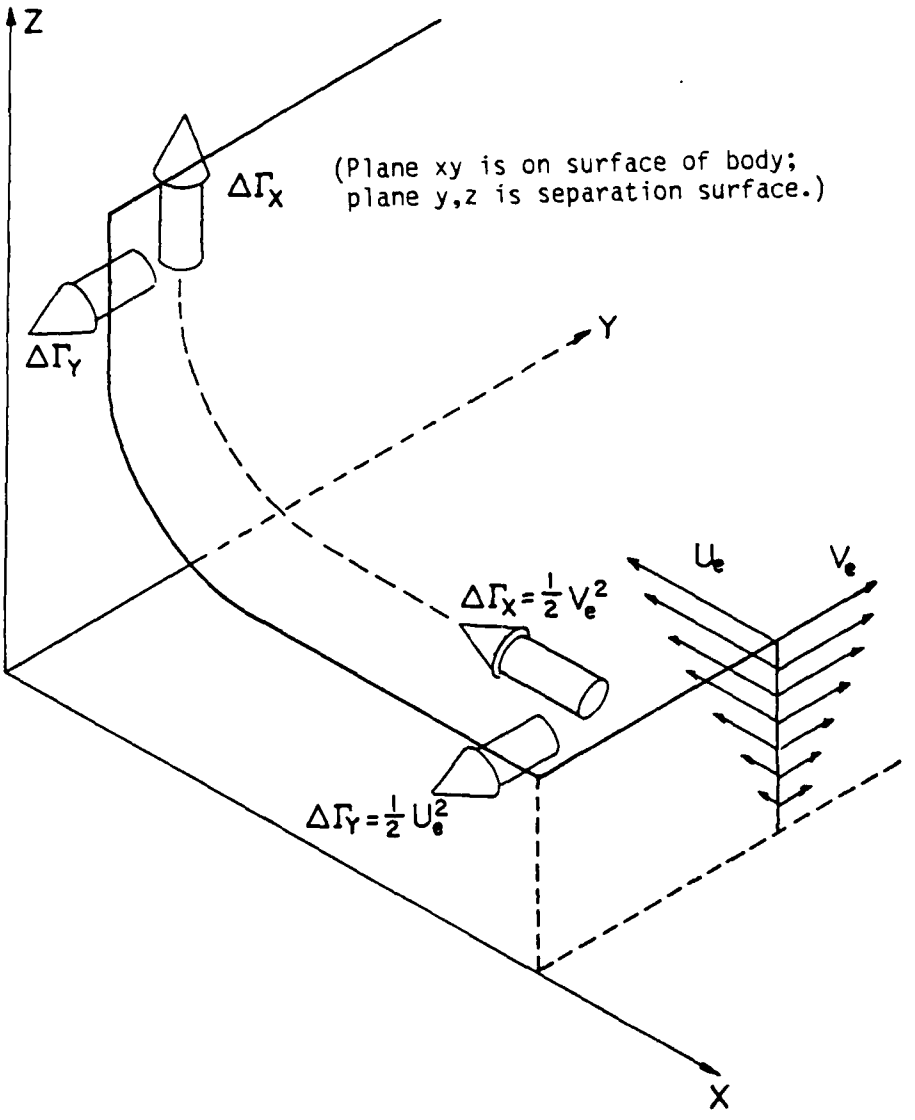

Fig. 8 Boundary layer and total vorticity flux near separation.

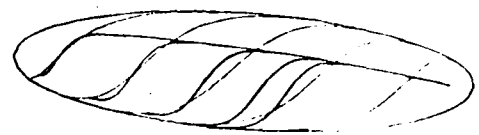

Fig. 9a - t = 0

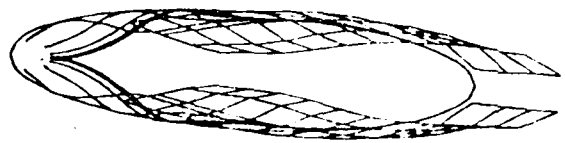

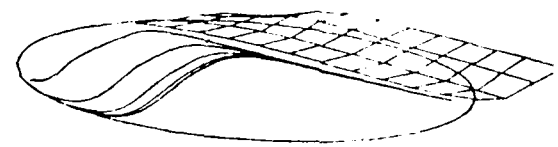

Fig. 9b - t = 3Δt

Fig. 9 Skin friction lines, separation and separated vortex sheets over a prolate spheroid started impulsively from rest.

Fig. 9 (continued)

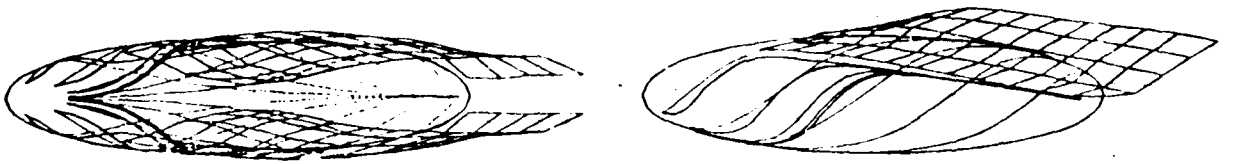

Fig 9c - t = 4Δt

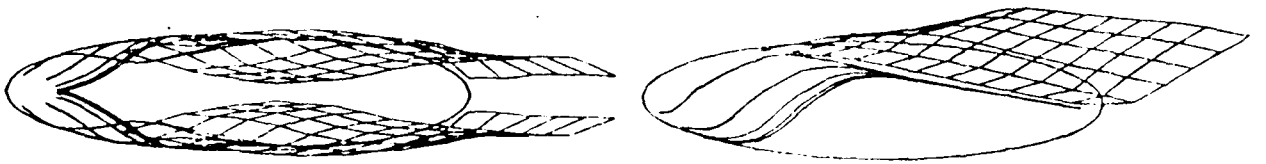

Fig. 9d - t = 5Δt

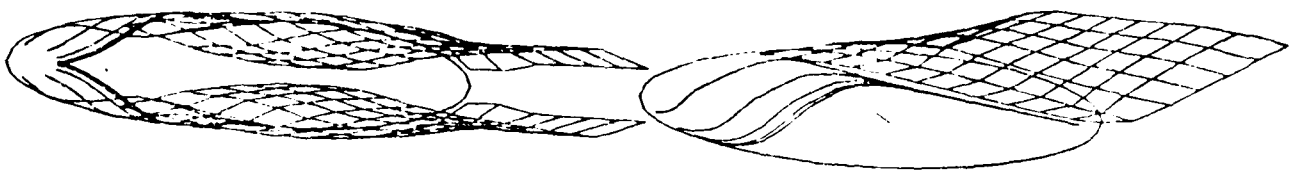

Fig. 9e - t = 6Δt

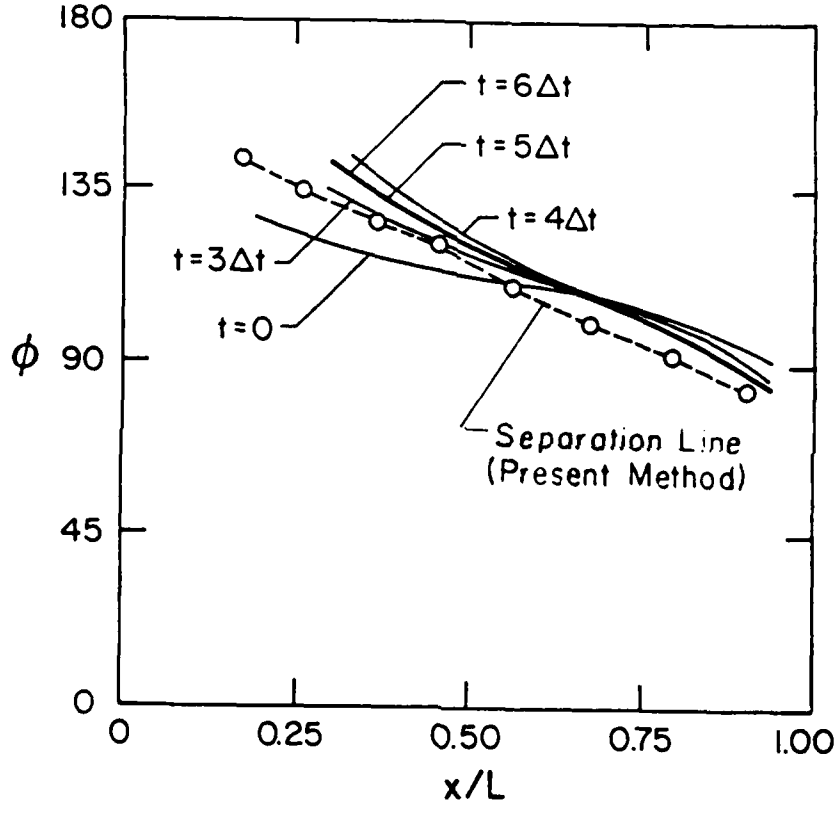

Fig. 10 The instantaneous line of separation for a prolate spheroid started impulsively from rest.

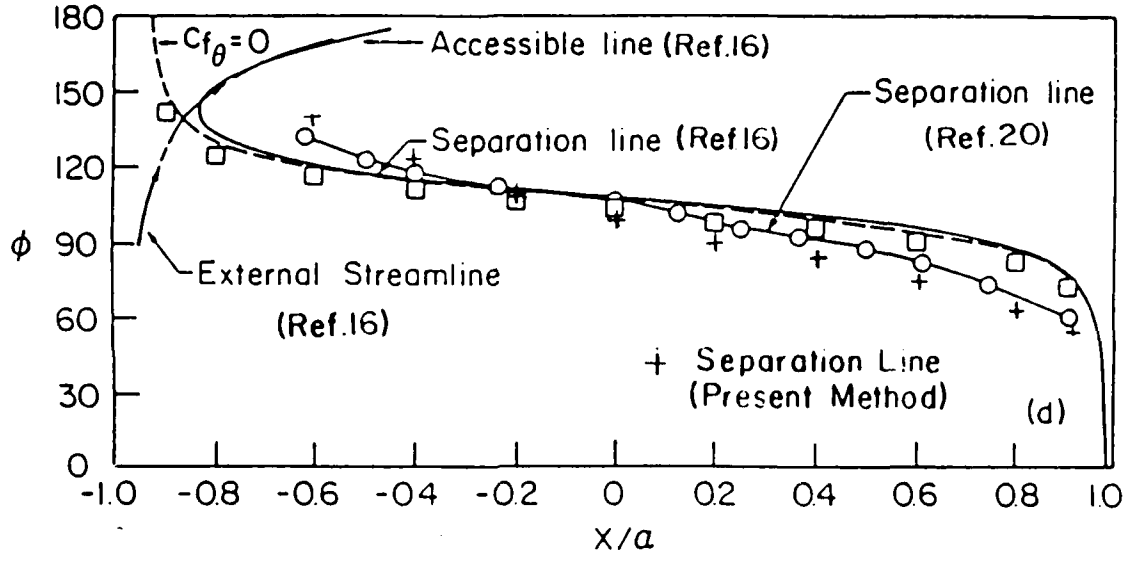

Fig. 11 Lines of separation and external streamlines for a prolate spheroid of a/b = 4 at an angle of attack a = 30°.

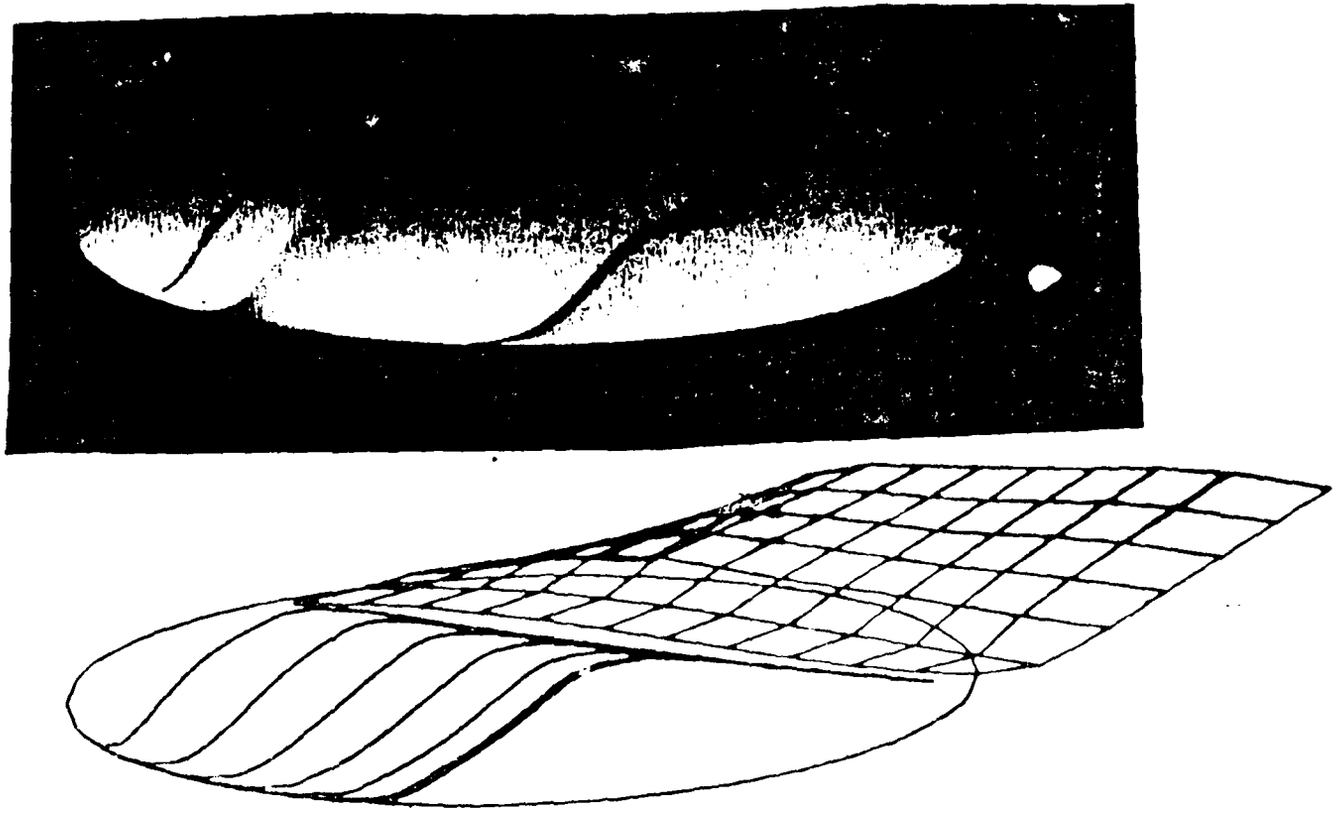

Fig. 12 Comparison of flow visualizations from Ref. 20 with present calculations at $\phi = 90°$.

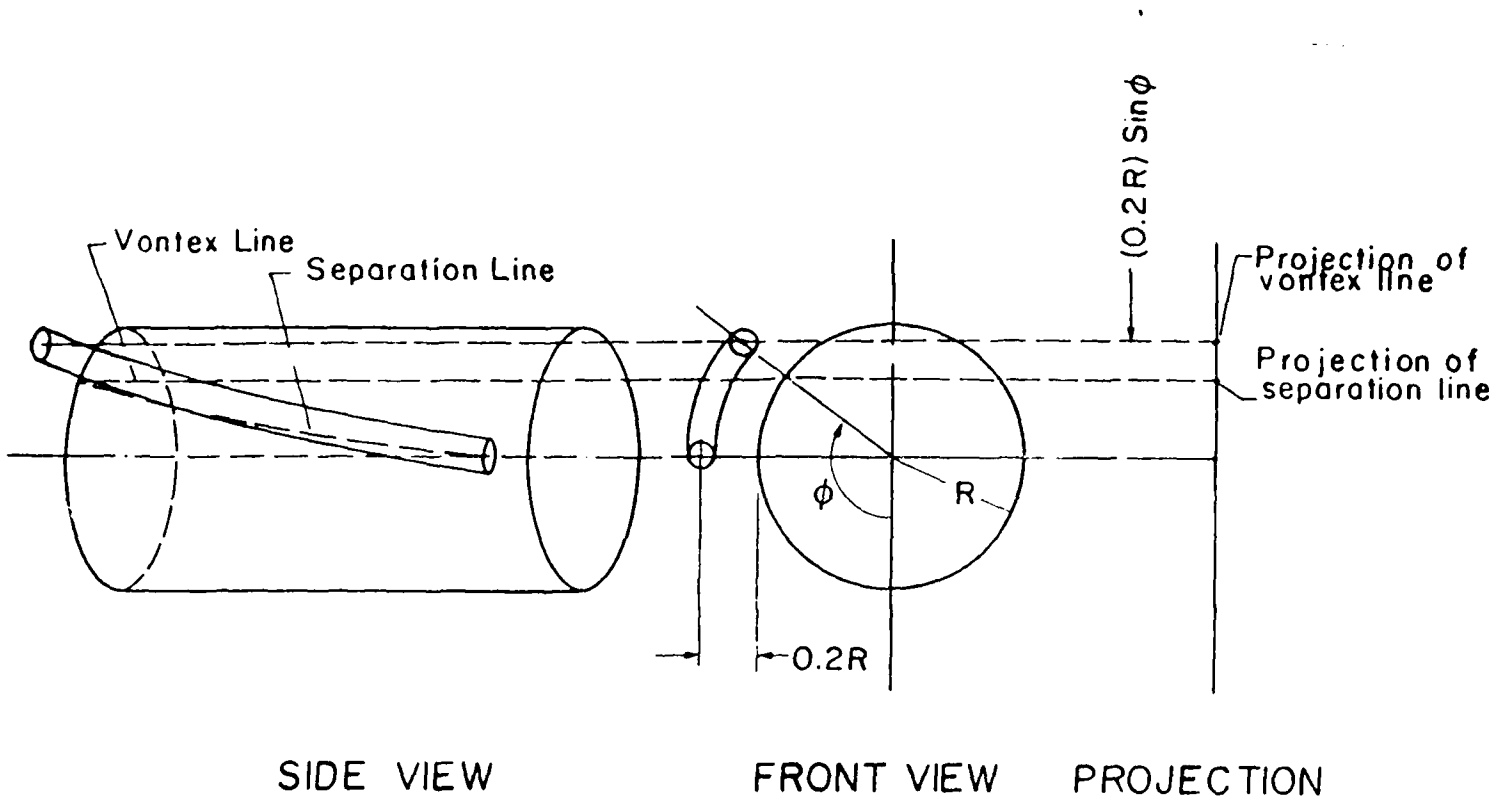

Fig. 13 Schematic representation showing a vortex line off the surface of the body.

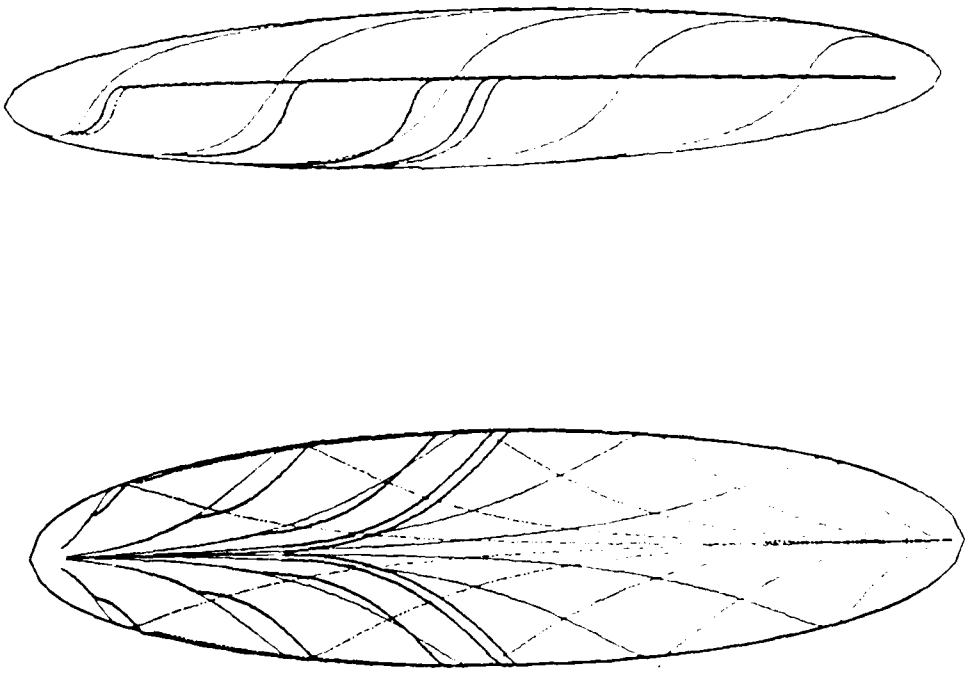

Fig. 14a Skin friction and potential lines of an ellipsoid with axes ratio 1:6:4

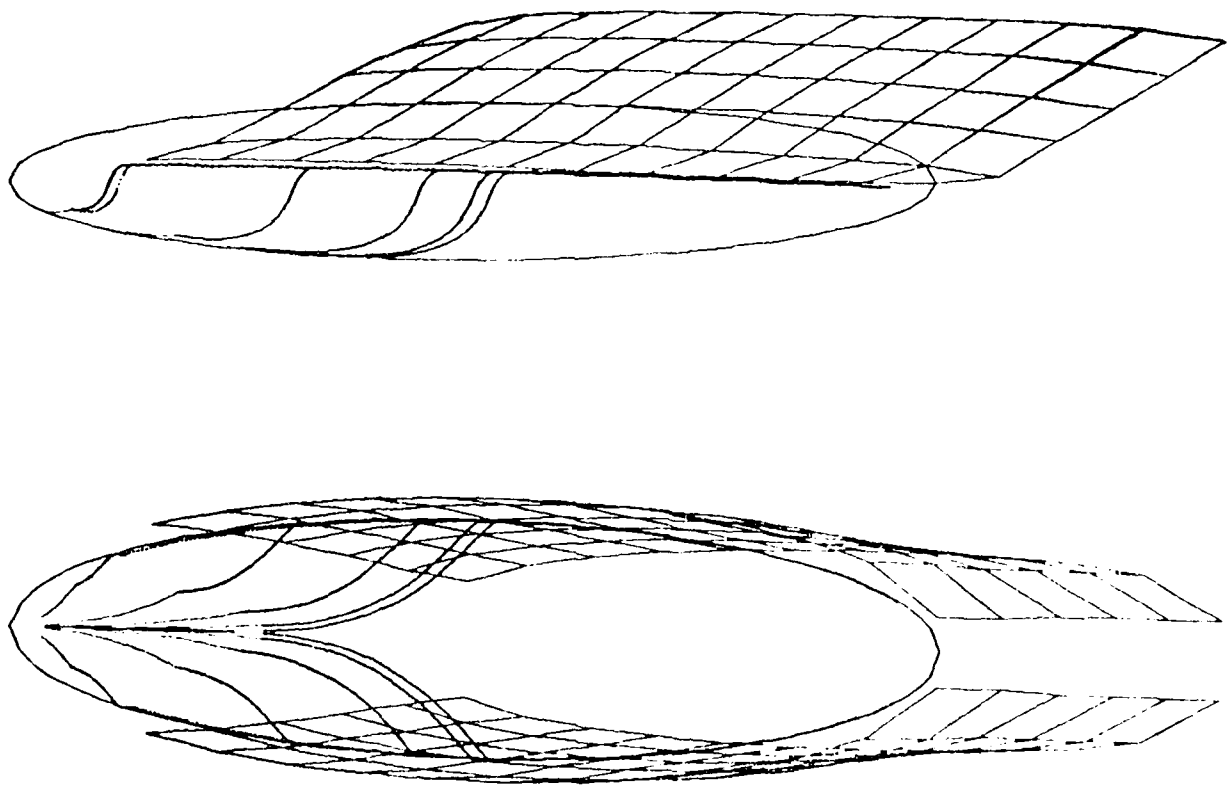

Fig. 14b Skin friction lines, potential ines and separated vortex sheets over an ellipsoid with axes ratio 1:6:4 started impulsively from rest at an angle of attack, $\alpha = 30°$.

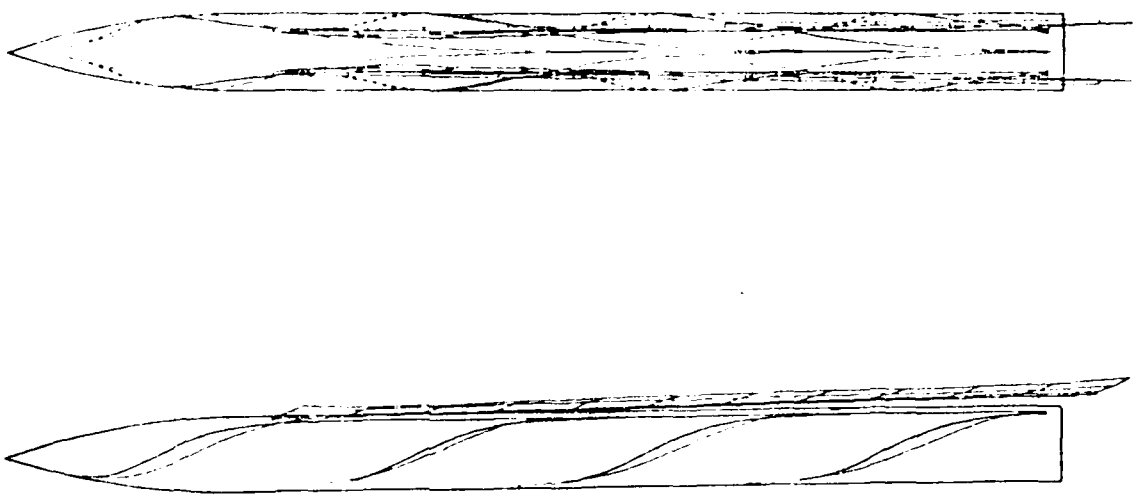

Fig. 15 Skin friction lines, potential lines and separated vortex sheets over an ogive-cylinder body started impulsively from rest at an angle of attack, $\alpha = 24.5^{\circ}$.

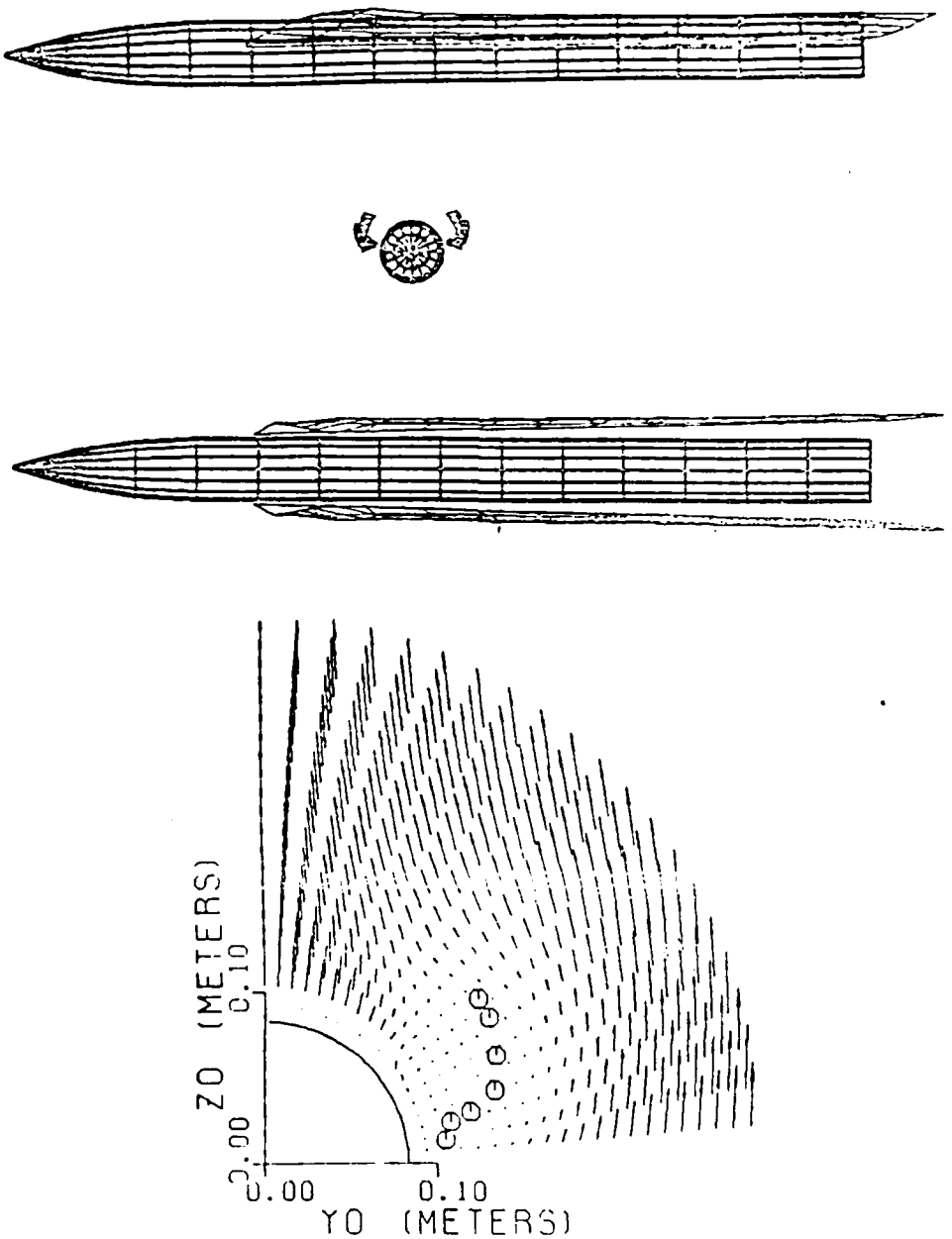

Fig. 16 Results for the body of Fig. 5.15 but with separation line fixed along a generator of the body.

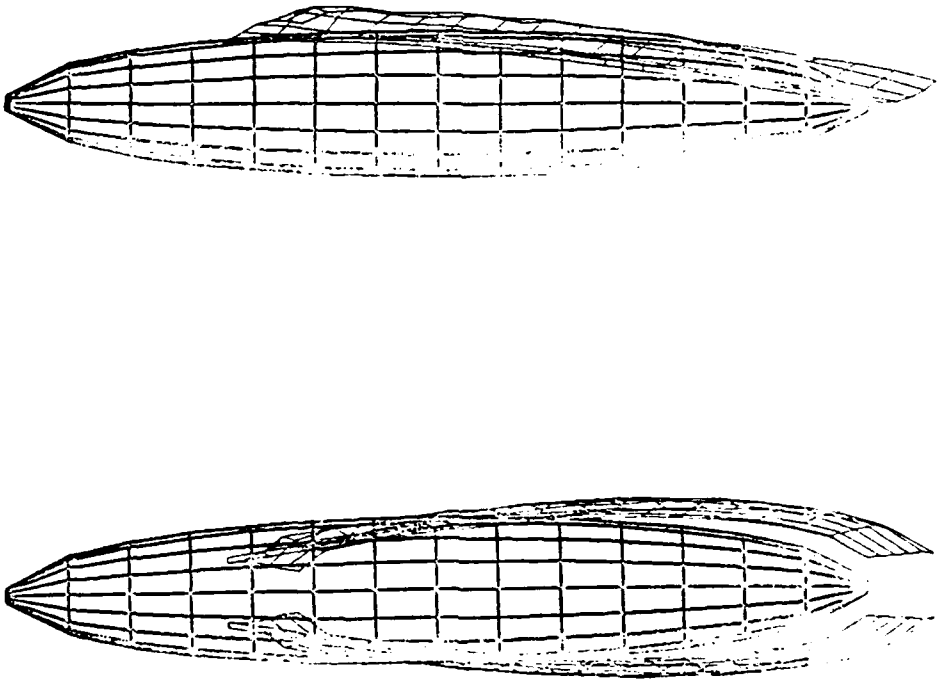

Fig. 17 The wake over a prolate spheroid with axes ratio 1:4 and the separation line fixed according to Meier's data.

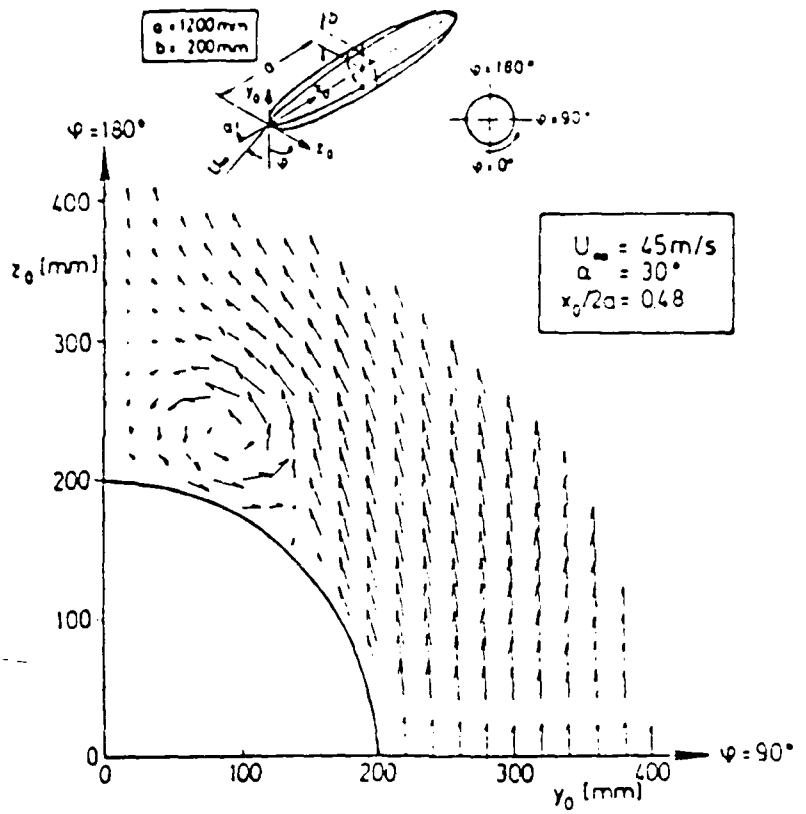

Fig. 18a Experiment, Ref. 26

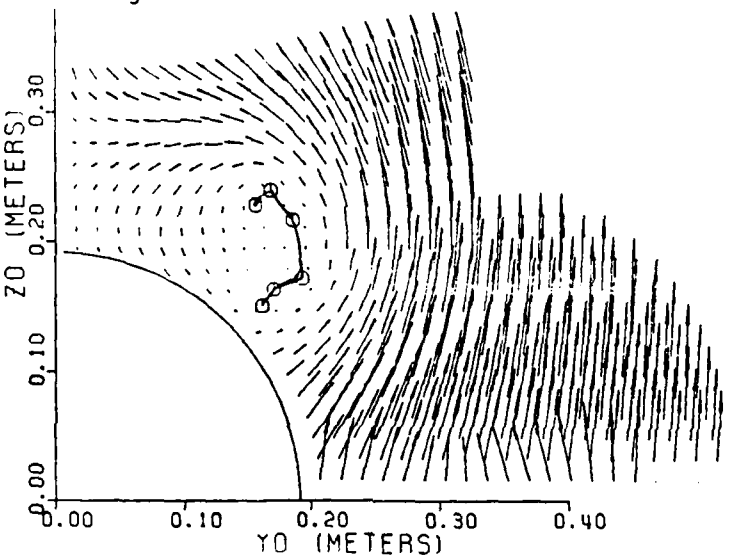

Fig. 18b Present theory

Fig. 18 Comparison of vector fields at a cross-sectional plane of x = 0.72.

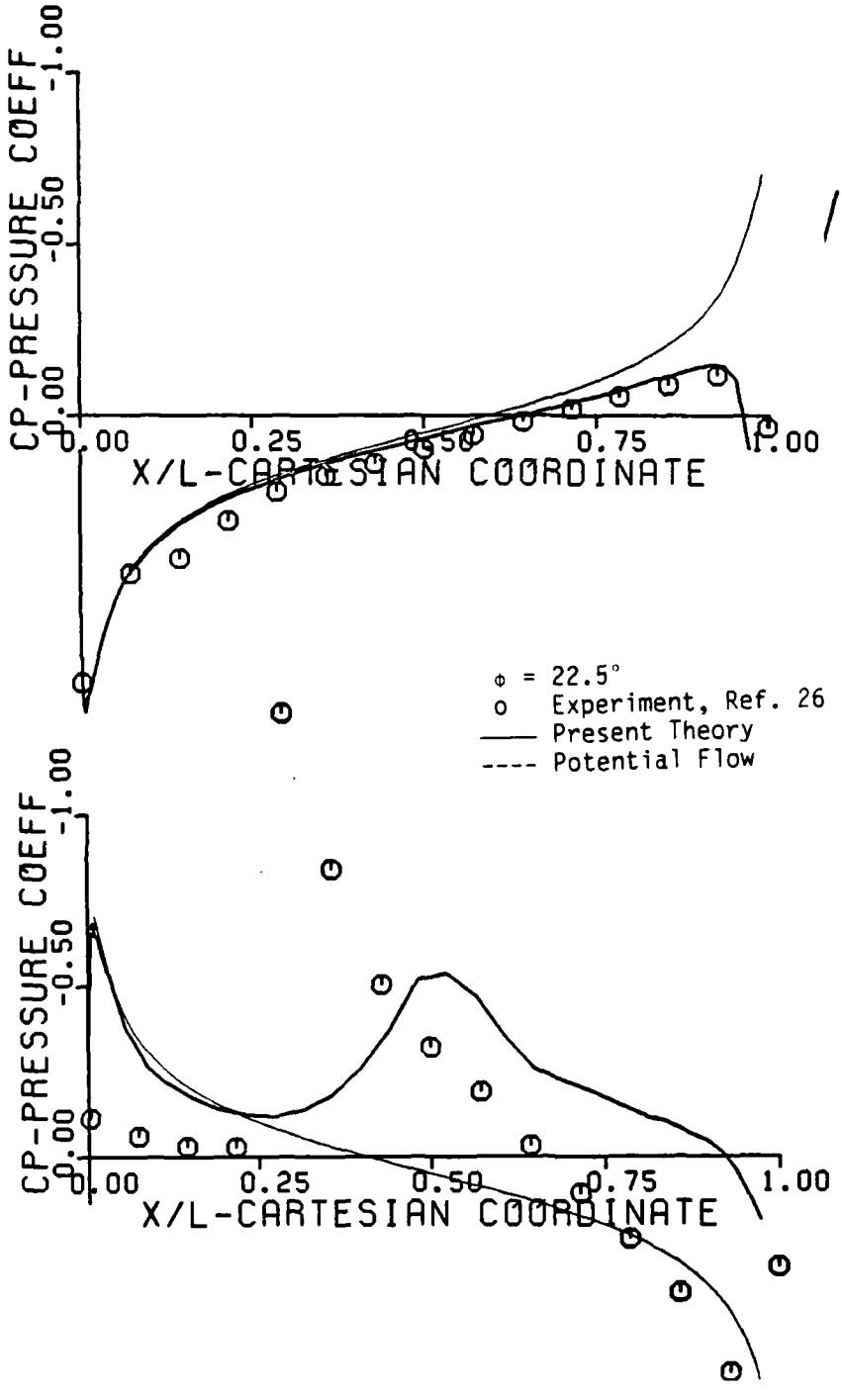

Fig. 19 Experimental and analytical pressure distributions for the case of Fig. 17.

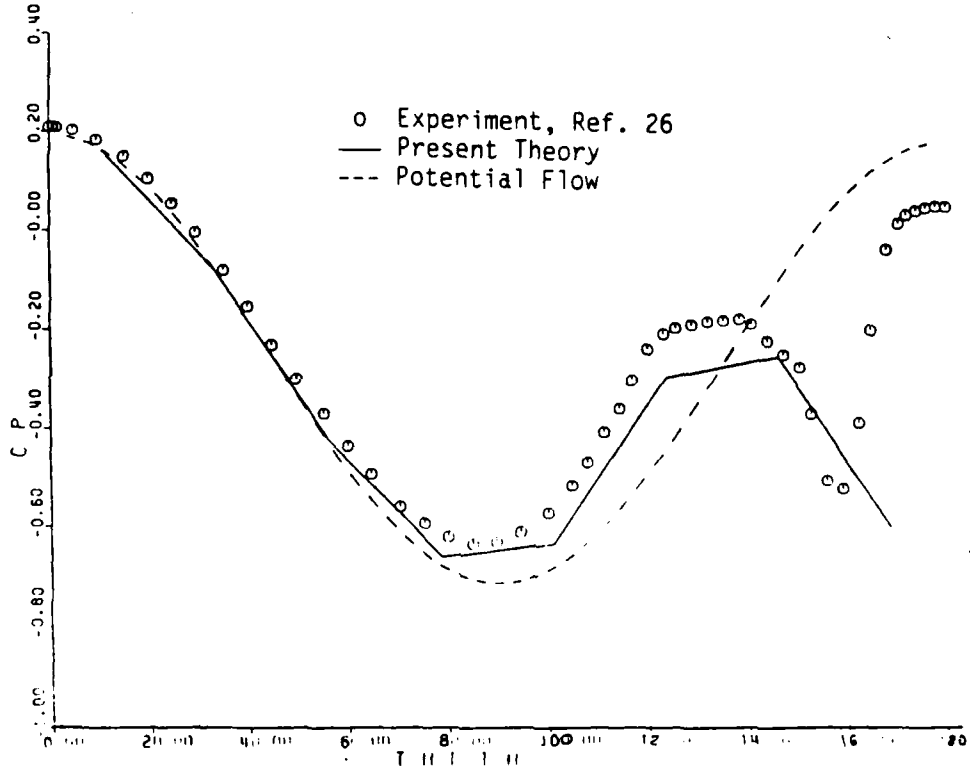

Fig. 20 Experimental and analytical pressure distribution for the case of Fig. 17, along the axial location x/L = 0.4812.

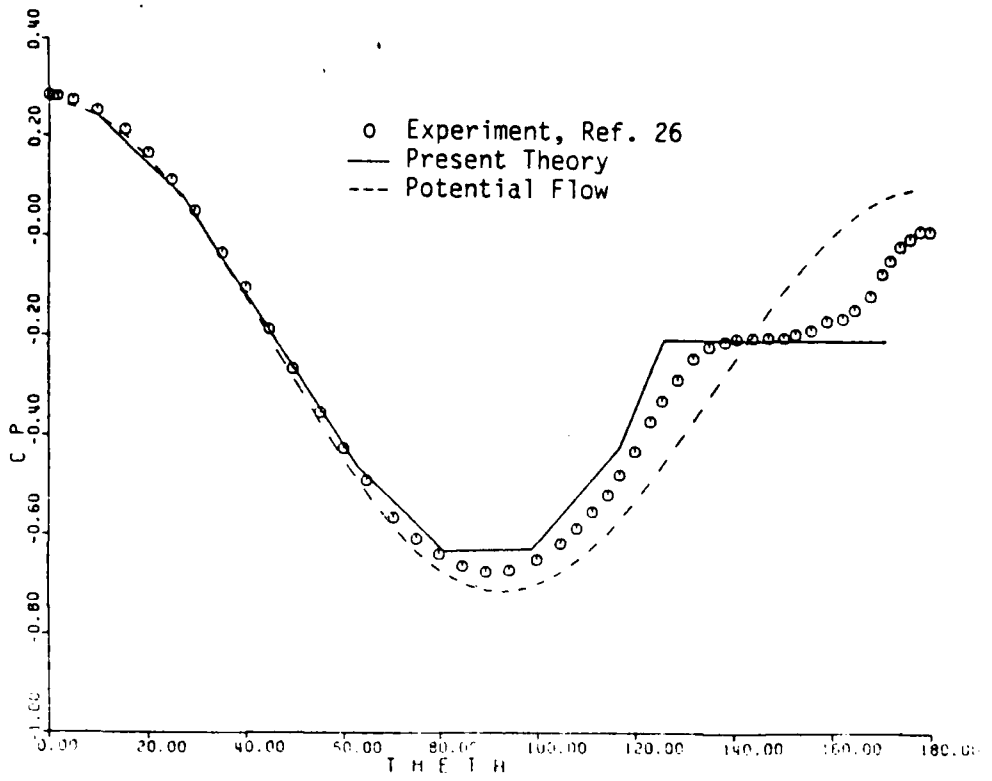

Fig. 21 Experimental and analytical pressure distribution for the case of Fig. 17, along the axial location x/L = 0.3501.

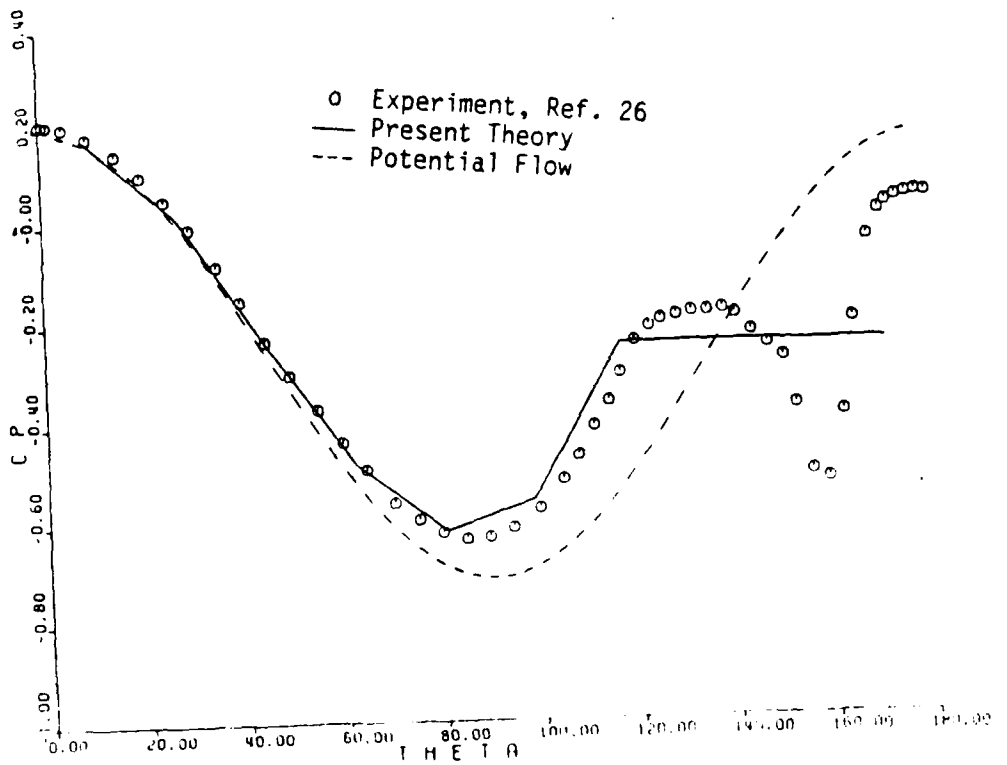

Fig. 22 Experimental and analytical pressure distribution for the case of Fig. 17, along the axial location x/L = 0.4812.

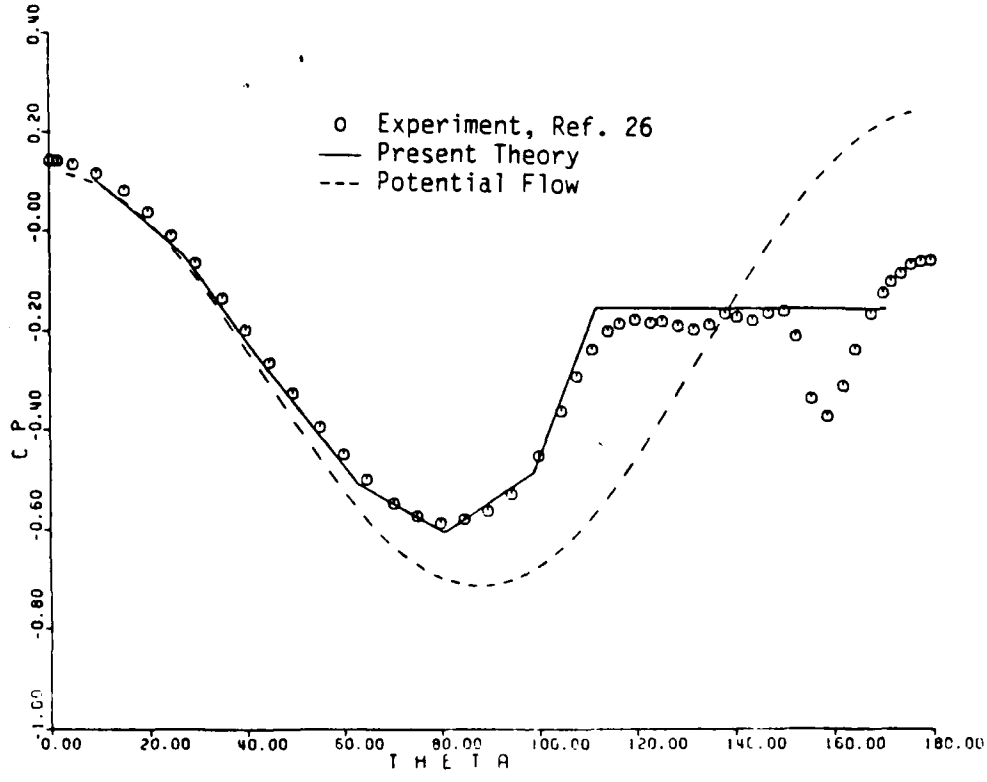

Fig. 23 Experimental and analytical pressure distribution for the case of Fig. 17, along the axial location x/L = 0.6061.

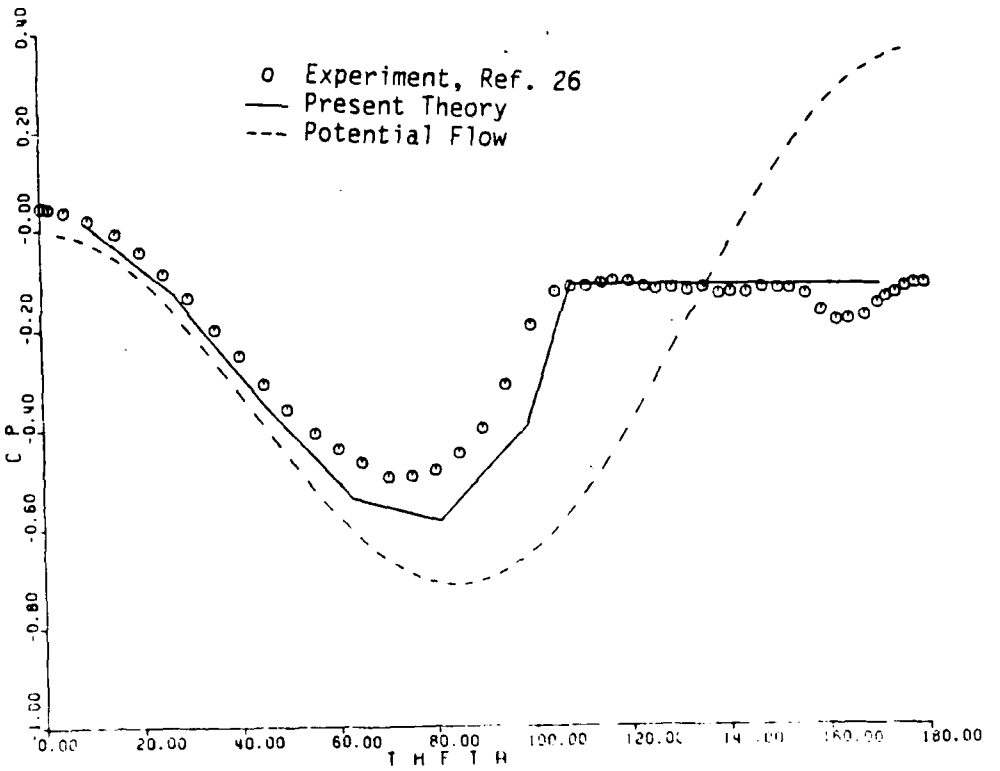

Fig. 24 Experimental and analytical pressure distribution for the case of Fig. 17, along the axial location x/L = 0.7725.

END

FILMED

4-86

DTIC